An ultrathin terahertz quarter-wave plate using planar babinet-inverted metasurface

Dacheng Wang,[1,2] Yinghong Gu,[1] Yandong Gong,[2] Cheng-Wei Qiu,[1] and Minghui Hong[1,*]

[1]*Department of Electrical and Computer Engineering, National University of Singapore, 4 Engineering Drive 3, Singapore 117581, Singapore*

[2]*Institute of Infocomm Research, 1 Fusionoplis Way, #21-01 Connexis, Singapore 13863, Singapore*

[*]*elehmh@nus.edu.sg*

Abstract: Metamaterials promise an exotic approach to artificially manipulate the polarization state of electromagnetic waves and boost the design of polarimetric devices for sensitive detection, imaging and wireless communication. Here, we present the design and experimental demonstration of an ultrathin (0.29λ) terahertz quarter-wave plate based on planar babinet-inverted metasurface. The quarter-wave plate consisting of arrays of asymmetric cross apertures reveals a high transmission of 0.545 with 90 degrees phase delay at 0.870 THz. The calculated ellipticity indicates a high degree of polarization conversion from linear to circular polarization. With respect to different incident polarization angles, left-handed circular polarized light, right-handed circular polarized light and elliptically polarized light can be created by this novel design. An analytical model is applied to describe transmitted amplitude, phase delay and ellipticitiy, which are in good agreement with the measured and simulated results. The planar babinet-inverted metasurface with the analytical model opens up avenues for new functional terahertz devices design.

OCIS codes: (160.3918) Metamaterials; (300.6495) Spectroscopy, terahertz; (260.1440) Birefringence.

References and Links

1. R. A. Shelby, D. R. Smith, and S. Schultz, "Experimental verification of a negative index of refraction," Science **292**(5514), 77–79 (2001).
2. D. R. Smith, W. J. Padilla, D. C. Vier, S. C. Nemat-Nasser, and S. Schultz, "Composite medium with simultaneously negative permeability and permittivity," Phys. Rev. Lett. **84**(18), 4184–4187 (2000).
3. J. B. Pendry, "Negative refraction makes a perfect lens," Phys. Rev. Lett. **85**(18), 3966–3969 (2000).
4. C. W. Qiu, L. Hu, X. Xu, and Y. Feng, "Spherical cloaking with homogeneous isotropic multilayered structures," Phys. Rev. E Stat. Nonlin. Soft Matter Phys. **79**(4), 047602 (2009).
5. D. Schurig, J. J. Mock, B. J. Justice, S. A. Cummer, J. B. Pendry, A. F. Starr, and D. R. Smith, "Metamaterial electromagnetic cloak at microwave frequencies," Science **314**(5801), 977–980 (2006).
6. X. L. Ma, W. B. Pan, C. Huang, M. B. Pu, Y. Q. Wang, B. Zhao, J. H. Cui, C. T. Wang, and X. G. Luo, "An active metamaterial for polarization manipulating," Adv. Opt. Mater. **2**(10), 945–949 (2014).
7. H. Li, L. H. Yuan, B. Zhou, X. P. Shen, Q. Cheng, and T. J. Cui, "Ultrathin multiband gigahertz metamaterial absorbers," J. Appl. Phys. **110**(1), 014909 (2011).
8. C. Zaichun, M. Rahmani, G. Yandong, C. T. Chong, and H. Minghui, "Realization of variable three-dimensional terahertz metamaterial tubes for passive resonance tunability," Adv. Mater. **24**(23), OP143–OP147 (2012).
9. S. Xiao, V. P. Drachev, A. V. Kildishev, X. Ni, U. K. Chettiar, H. K. Yuan, and V. M. Shalaev, "Loss-free and active optical negative-index metamaterials," Nature **466**(7307), 735–738 (2010).
10. M. J. Dicken, K. Aydin, I. M. Pryce, L. A. Sweatlock, E. M. Boyd, S. Walavalkar, J. Ma, and H. A. Atwater, "Frequency tunable near-infrared metamaterials based on VO2 phase transition," Opt. Express **17**(20), 18330–18339 (2009).
11. H. T. Chen, W. J. Padilla, J. M. O. Zide, A. C. Gossard, A. J. Taylor, and R. D. Averitt, "Active terahertz metamaterial devices," Nature **444**(7119), 597–600 (2006).
12. D. C. Wang, Q. Huang, C. W. Qiu, and M. H. Hong, "Selective excitation of resonances in gammadion metamaterials for terahertz wave manipulation," Sci. China: Phys., Mech. Astron. **58**, 084201 (2015).

#233466 - $15.00 USD Received 29 Jan 2015; revised 11 Apr 2015; accepted 15 Apr 2015; published 21 Apr 2015

13. L. Q. Cong, W. Cao, X. Q. Zhang, Z. Tian, J. Q. Gu, R. Singh, J. G. Han, and W. L. Zhang, "A perfect metamaterial polarization rotator," Appl. Phys. Lett. **103**(17), 171107 (2013).
14. W. M. Zhu, H. Cai, T. Mei, T. Bourouina, J. F. Tao, G. Q. Lo, D. L. Kwong, and A. Q. Liu, "A MEMS tunable metamaterial filter," Proc. IEEE Micr. Elect. Jan 24–28, pp.196–199 (2010).
15. X. P. Shen and T. J. Cui, "Photoexcited broadband redshift switch and strength modulation of terahertz metamaterial absorber," J. Opt. **14**(11), 114012 (2012).
16. A. Benz, M. Krall, S. Schwarz, D. Dietze, H. Detz, A. M. Andrews, W. Schrenk, G. Strasser, and K. Unterrainer, "Resonant metamaterial detectors based on THz quantum-cascade structures," Sci. Rep. **4**, 4269 (2014).
17. K. Wiesauer and C. Jordens, "Recent Advances in Birefringence Studies at THz Frequencies," J. Infrared, Millimeter, Terahertz Waves **34**(11), 663–681 (2013).
18. G. Kenanakis, R. Zhao, N. Katsarakis, M. Kafesaki, C. M. Soukoulis, and E. N. Economou, "Optically controllable THz chiral metamaterials," Opt. Express **22**(10), 12149–12159 (2014).
19. S. Zhang, J. Zhou, Y. S. Park, J. Rho, R. Singh, S. Nam, A. K. Azad, H. T. Chen, X. Yin, A. J. Taylor, and X. Zhang, "Photoinduced handedness switching in terahertz chiral metamolecules," Nat. Commun. **3**, 942–948 (2012).
20. A. V. Rogacheva, V. A. Fedotov, A. S. Schwanecke, and N. I. Zheludev, "Giant gyrotropy due to electromagnetic-field coupling in a bilayered chiral structure," Phys. Rev. Lett. **97**(17), 177401 (2006).
21. R. Singh, E. Plum, C. Menzel, C. Rockstuhl, A. K. Azad, R. A. Cheville, F. Lederer, W. Zhang, and N. I. Zheludev, "Terahertz metamaterial with asymmetric transmission," Phys. Rev. B **80**(15), 153104 (2009).
22. R. Singh, E. Plum, W. Zhang, and N. I. Zheludev, "Highly tunable optical activity in planar achiral terahertz metamaterials," Opt. Express **18**(13), 13425–13430 (2010).
23. J. M. Hao, Q. J. Ren, Z. H. An, X. Q. Huang, Z. H. Chen, M. Qiu, and L. Zhou, "Optical metamaterial for polarization control," Phys. Rev. A **80**(2), 023807 (2009).
24. J. Hao, Y. Yuan, L. Ran, T. Jiang, J. A. Kong, C. T. Chan, and L. Zhou, "Manipulating electromagnetic wave polarizations by anisotropic metamaterials," Phys. Rev. Lett. **99**(6), 063908 (2007).
25. L. Q. Cong, N. N. Xu, J. Q. Gu, R. Singh, J. G. Han, and W. L. Zhang, "Highly flexible broadband terahertz metamaterial quarter-wave plate," Laser Photonics Rev. **8**(4), 626–632 (2014).
26. N. K. Grady, J. E. Heyes, D. R. Chowdhury, Y. Zeng, M. T. Reiten, A. K. Azad, A. J. Taylor, D. A. R. Dalvit, and H. T. Chen, "Terahertz metamaterials for linear polarization conversion and anomalous refraction," Science **340**(6138), 1304–1307 (2013).
27. N. Yu, P. Genevet, M. A. Kats, F. Aieta, J. P. Tetienne, F. Capasso, and Z. Gaburro, "Light propagation with phase discontinuities: Generalized laws of reflection and refraction," Science **334**(6054), 333–337 (2011).
28. F. Falcone, T. Lopetegi, M. A. G. Laso, J. D. Baena, J. Bonache, M. Beruete, R. Marqués, F. Martín, and M. Sorolla, "Babinet principle applied to the design of metasurfaces and metamaterials," Phys. Rev. Lett. **93**(19), 197401 (2004).
29. N. Meinzer, W. L. Barnes, and I. R. Hooper, "Plasmonic meta-atoms and metasurfaces," Nat. Photonics **8**(12), 889–898 (2014).
30. D. Lin, P. Fan, E. Hasman, and M. L. Brongersma, "Dielectric gradient metasurface optical elements," Science **345**(6194), 298–302 (2014).
31. C. García-Meca, R. Ortuño, F. J. Rodríguez-Fortuño, J. Martí, and A. Martínez, "Negative refractive index metamaterials aided by extraordinary optical transmission," Opt. Express **17**(8), 6026–6031 (2009).
32. W. C. Chen, N. I. Landy, K. Kempa, and W. J. Padilla, "A subwavelength extraordinary-optical-transmission channel in Babinet metamaterials," Adv. Opt. Mater. **1**(3), 221–226 (2013).
33. M. Navarro-Cía, M. Beruete, I. Campillo, and M. Sorolla, "Enhanced lens by ε and μ near-zero metamaterial boosted by extraordinary optical transmission," Phys. Rev. B **83**(11), 115112 (2011).
34. T. Li, H. Liu, S. M. Wang, X. G. Yin, F. M. Wang, S. N. Zhu, and X. A. Zhang, "Manipulating optical rotation in extraordinary transmission by hybrid plasmonic excitations," Appl. Phys. Lett. **93**(2), 021110 (2008).
35. W. Sun, Q. He, J. Hao, and L. Zhou, "A transparent metamaterial to manipulate electromagnetic wave polarizations," Opt. Lett. **36**(6), 927–929 (2011).
36. M. Zalkovskij, R. Malureanu, C. Kremers, D. N. Chigrin, A. Novitsky, S. Zhukovsky, P. T. Tang, P. U. Jepsen, and A. V. Lavrinenko, "Optically active Babinet planar metamaterial film for terahertz polarization manipulation," Laser Photonics Rev. **7**(5), 810–817 (2013).
37. T. Xu, C. L. Du, C. T. Wang, and X. G. Luo, "Subwavelength imaging by metallic slab lens with nanoslits," Appl. Phys. Lett. **91**(20), 201501 (2007).
38. T. Xu, C. Wang, C. Du, and X. Luo, "Plasmonic beam deflector," Opt. Express **16**(7), 4753–4759 (2008).
39. H. Dong, Y. D. Gong, V. Paulose, and M. H. Hong, "Polarization state and Mueller matrix measurements in terahertz-time domain spectroscopy," Opt. Commun. **282**(18), 3671–3675 (2009).
40. Z. C. Chen, Y. D. Gong, H. Dong, T. Notake, and H. Minamide, "Terahertz achromatic quarter wave plate: Design, fabrication, and characterization," Opt. Commun. **311**, 1–5 (2013).
41. J. B. Masson and G. Gallot, "Terahertz achromatic quarter-wave plate," Opt. Lett. **31**(2), 265–267 (2006).
42. D. Goldstein, *Polarized Light* 2nd ed. (Marcel Dekker, 2003).
43. J. H. Choe, J. H. Kang, D. S. Kim, and Q. H. Park, "Slot antenna as a bound charge oscillator," Opt. Express **20**(6), 6521–6526 (2012).

#233466 - $15.00 USD Received 29 Jan 2015; revised 11 Apr 2015; accepted 15 Apr 2015; published 21 Apr 2015

1. Introduction

Metamaterials, artificial sub-wavelength scale structures, have attracted a great deal of research attentions due to their possibilities to engineer optical properties which cannot be obtained in nature materials, such as negative index [1, 2], perfect lens [3] and cloaking [4, 5]. Over the last few decades, a variety of functional metamaterial designs have been demonstrated to manipulate electromagnetic waves across the whole spectrum from microwave to visible light [6–10]. This is especially important in terahertz (THz) frequency range because many natural materials present weak response to THz wave, making it hard to construct THz devices. To bridge this gap, people have recently proposed a wide range of metamaterials based THz devices to control THz wave, such as modulators [11, 12], polarizers [13], filters [14], absorbers [15] and detectors [16].

In particular, manipulation of polarization state in THz range is of great importance because information conveyed by the polarization state promises applications for sensitive detection of explosive materials, THz imaging and THz wireless communication. Conventional approaches to manipulate the polarization of THz wave depend on the properties of birefringent materials [17], which have many limitations, such as limited available materials, bulky volume, high loss, specific device thickness and narrow band operation frequency. Recently, researchers have demonstrated THz polarization manipulation devices based on various metamaterial designs. Chiral metamaterials, as an analog of chiral molecules, are widely adopted to control THz polarization. Most of the demonstrated chiral metamaterials are complex with multilayer or 3D design [18–20]. These metamaterials need precise alignment fabrication techniques and their integration into a THz-optic system is challenging. On the other hand, simple geometric metamaterials have been investigated recently for THz polarization control, such as planar chiral structures [21], planar nonchiral metamaterials [22–24] and multilayer metamaterials [25, 26]. These designs are composed of periodic sub-wavelength metallic structures, which act as band stop resonators. The transmitted amplitude is small when THz wave interacts with these resonators. To overcome this issue, the majority of metamaterial designs are multilayers because multireflection among different layers can enhance the transmission coefficient [26]. Another approach is to design metasurface-based devices for polarization and phase modulation. In 2011, Capasso et al demonstrated the control of phase shift through a nano-antenna array [27]. Although the thickness is decreased to tens of nanometers, the phase shift is accompanied with polarization conversion, which would limit their practical applications. Babinet-inverted metasurfaces attract prominent research attentions recently because they are band pass resonators with an ultrathin device thickness and a maximum transmission at the resonance [28, 29]. The transmitted amplitude and phase of the metasurface can be manipulated by controlling the size, geometry, materials and relative orientations of the resonators [29, 30]. Extraordinary optical transmission (EOT) in babinet-inverted metasurface has been reported at different frequency regimes [31–35]. Meanwhile, the babinet-inverted metasurface only enables the resonant electromagnetic wave to pass through. It can be a free-standing metasurface, which eliminates optical losses due to substrates [36].

In this work, we demonstrate an ultrathin THz quarter wave plate (QWP) for polarization control based on planar babinet-inverted metasurface. The quarter wave plate is constructed by arrays of asymmetric metallic cross apertures, which can support two orthogonal resonant modes in THz range. Each resonant mode gives rise to extraordinary optical transmission accompanied by a specific phase shift at the resonance. According to the dispersion equation of surface plasmon in metallic slots, the propagation constants as well as the phase delays are tunable by varying the width and length of the slots [37, 38]. By properly choosing the size of the asymmetric cross aperture, two resonant modes superpose with each other, producing equal transmitted amplitudes with a phase difference of 90 degrees at a certain frequency and operating as a THz quarter wave plate. When the incident polarization angle changes, the

#233466 - $15.00 USD Received 29 Jan 2015; revised 11 Apr 2015; accepted 15 Apr 2015; published 21 Apr 2015

transmitted THz wave can be elliptically polarized with an ellipticity from 1 to −1. A simple Lorentz oscillator model is employed to analytically describe the performance of the quarter wave plate, which is in good agreement with our experimental and simulation results.

2. Design and fabrication

The unit cell of the babinet-inverted resonator arrays is schematically shown in Fig. 1(a), which consists of two slots perpendicular to each other in a copper film. The lengths of two slots are lx = 105 μm and ly = 125 μm, respectively. The width of both slots is w = 6 μm. The periodicity of the babinet-inverted resonator arrays is P = 150 μm. The copper film is 200 nm thick deposited on a flexible polyethylene naphthalate (PEN) film, which is transparent to THz wave at a thickness of 100 μm. When THz wave polarized at θ = 45 degrees to x-axis is normally irradiated on the two slots, two resonant modes inside the slots can be excited simultaneously, resulting in the same transmitted amplitudes along both x- and y- axes with 90 degrees phase delay at a certain frequency. Therefore, the device operates as a QWP, converting a linearly polarized light into a circular polarized light as shown in Fig. 1(b).

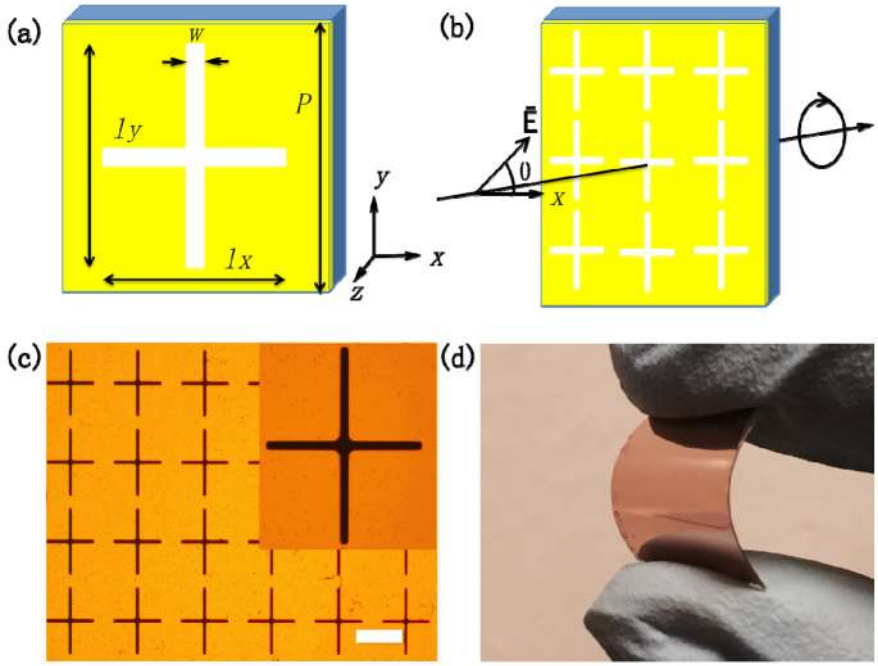

Fig. 1. (a) Schematic of one unit cell. (b) Schematic of working principle of the QWP. The normal incident THz wave is polarized at θ = 45 degrees to x-axis. (c) Microscope image of the fabricated asymmetric cross apertures with a zoomed image as the insert. The scale bar is 100 μm. (d) Photograph of the fabricated THz QWP.

The THz QWP was fabricated on the PEN film by photolithography. First, positive photoresist S1813 was coated onto the PEN film by a spin coater at a spin speed of 3000 rmp for 30 s, followed by hot plate baking at 110 °C for 1 minute. The asymmetric cross shape was defined on photoresist surface by photolithography (MA6, Karl Suss). After photoresist development in MF319 for 1 minute, an adhesion layer of 5 nm thick chromium was coated on the samples followed by depositing 200 nm thick copper in a thermal evaporator (Edwards Auto 306). The last step to pattern the designed structure was a lift-off process in the acetone. The microscope image of the fabricated asymmetric cross aperture is shown in Fig. 1(c) with a zoomed image as the insert. The photograph of the fabricated sample is shown in Fig. 1(d), indicating its good flexibility.

#233466 - $15.00 USD Received 29 Jan 2015; revised 11 Apr 2015; accepted 15 Apr 2015; published 21 Apr 2015

3. Characterization and simulation

The THz QWP was characterized by a polarimetric THz time domain spectroscope (TDS) [39]. In this system, a 10 fs laser pulse with a center wavelength of 800 nm and a repetition rate of 80 MHz is split into two beams. One beam with an average power of 28 mW was focused onto the photoconductive antennas in the THz emitter for THz wave generation. The other beam with an average power of 32 mW was focused onto the photoconductive antennas in the THz detector to detect THz wave. A wire-grid THz polarizer is placed in front of the THz emitter for a linearly polarized input THz wave. Another wire-grid THz polarizer is positioned in front of the THz detector. Both polarizers can be rotated at any direction by the rotation stage, which is controlled by a computer, enabling us to measure the polarization states of the output THz wave.

The system is put inside a sealed purging box, which is filled with nitrogen gas to minimize water absorption in THz range. During the measurement, the incident THz wave was polarized at θ = 45 degrees to the two slots in the QWP. After transmitted through the QWP, electric field of THz wave was measured along *x*- and *y*-axes, which were denoted as $\bar{E}x$ and $\bar{E}y$. A bare PEN substrate was measured as a reference sample with transmitted electric field $\bar{E}x(ref)$ and $\bar{E}y(ref)$. The amplitude transmission of the QWP can be obtained as $|\tilde{t}x| = |\bar{E}x/\bar{E}x(ref)|$ and $|\tilde{t}y| = |\bar{E}y/\bar{E}y(ref)|$, which are shown in Fig. 2(a). The phase difference between two orthogonal slots was calculated from the measured data with $\varphi = \varphi_y - \varphi_x = \arg(\tilde{t}y) - \arg(\tilde{t}x)$, which is shown in Fig. 2(d). From the measured results, we can observe two resonant peaks at 0.806 and 0.925 THz, which correspond to fundamental resonant modes under *x*- and *y*- axes polarized incident light. The superposition of these two peaks presents an equal transmitted amplitude of ~0.545 at 0.870 THz along both *x*- and *y*- axes. The measured phase difference between *x*- and *y*- axes is around 90 degrees at 0.870 THz. This indicates that the incident linearly polarized THz wave is converted into a circular polarized THz wave at 0.870 THz. Our THz QWP has an ultrathin device thickness (100.2 μm ≈0.29λ, much thinner than commercial available birefringent materials based THz QWP of mm scale device thickness [40, 41]) with a high transmission (0.545) and good flexibility.

Numerical simulation was carried out by finite-difference time-domain (FDTD) method (FDTD Solutions 8.9, Lumerical Inc.) to confirm our measured results. The copper film in the QWP was treated as a lossy metal with an electrical conductivity of 5.8×10^7 *S/m* and the PEN substrate was modeled as a lossless dielectric with $\varepsilon_{pen} = 3.15$. The simulated amplitude transmission and phase difference are shown in Figs. 2(b) and 2(e). At 0.874 THz, transmitted amplitude of ~0.628 with a phase delay of around 90 degrees is presented, which is in good agreement with the measured results, indicating a good polarization conversion in our designed THz QWP. A small resonance frequency shift is observed between the experimental and simulation results, due to size fluctuation during our fabrication. The absolute amplitude difference between the simulation and experimental results corresponds to loss introduced in the metal film and PEN substrate.

In order to investigate the polarization state of the THz wave transmitted through the QWP, Stokes parameters were calculated based on the measured and simulated results [13, 25, 42]. As the incident THz wave is polarized at θ = 45 degrees to *x*-axis, the incident electric field can be noted as:

$$\overline{E} = \overline{E}_x + \overline{E}_y = \tilde{t}_x \cos\theta + \tilde{t}_y \sin\theta.$$

#233466 - $15.00 USD Received 29 Jan 2015; revised 11 Apr 2015; accepted 15 Apr 2015; published 21 Apr 2015

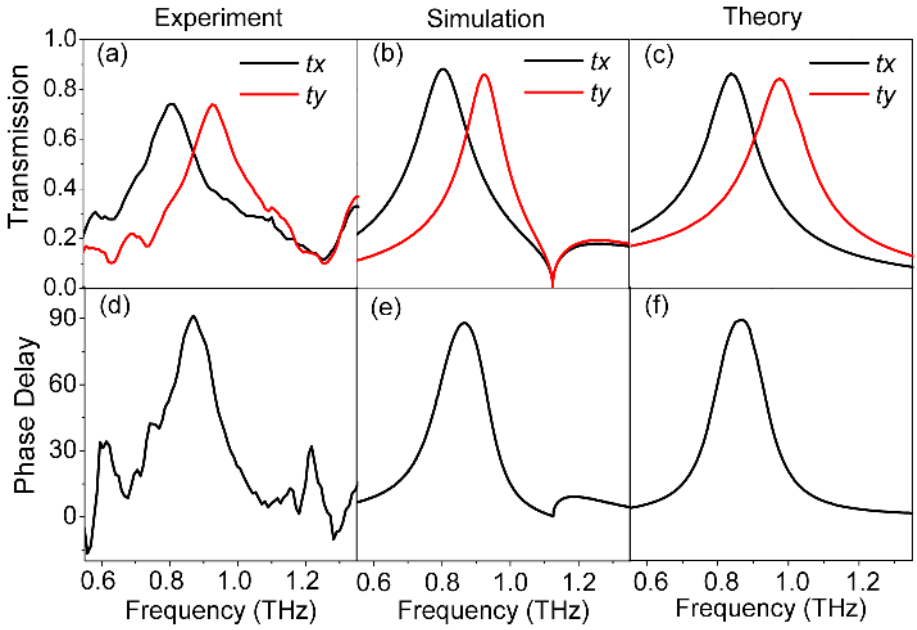

Fig. 2. (a) Measured, (b) numerical simulated and (c) analytical model calculated transmission and phase delay between two resonant modes for (d) experimental, (e) simulation and (f) theoretical results.

Therefore, Stokes parameters can be calculated as:

$$\begin{aligned} S_0 &= \left|\overline{E}_x\right|^2 + \left|\overline{E}_y\right|^2, \\ S_1 &= \left|\overline{E}_x\right|^2 - \left|\overline{E}_y\right|^2, \\ S_2 &= 2\left|\overline{E}_x\right|\left|\overline{E}_y\right|\cos\varphi, \\ S_3 &= 2\left|\overline{E}_x\right|\left|\overline{E}_y\right|\sin\varphi. \end{aligned} \tag{1}$$

Figures 3(a) and 3(b) show the measured and simulated S_0 parameters, which are the output electric field powers. At 0.870 THz, the QWP presents an output power of 0.297 in experiment, while in simulation the output power is 0.394 at 0.874 THz. The difference between experiment and simulation may be due to loss induced in the substrate and metal, which can be further improved by designing freestanding metal structures and optimizing parameters, such as decreasing the periodicity. Even though the output power is not high enough, the measured transmission amplitude of the electric field at 0.545 for our THz QWP is still quite applicable in a THz system. The ellipticity of the transmitted THz wave is defined as $\chi = S_3/ S_0$. When $\chi = 1$, the transmitted THz wave is a left-handed circular polarized (LCP) light and when $\chi = -1$, the transmitted THz wave is a right-handed circular polarized (RCP) light. The ellipticities calculated from our measured and simulated data are shown in Figs. 3(c) and 3(d). In the experiment, the ellipticity at 0.870 THz is $\chi = 1$, indicating the output THz wave is a perfect LCP light. The simulated ellipticity presents similar results with $\chi = 0.999$ at 0.874 THz. Therefore, this ultrathin device shows good performance as a THz QWP.

#233466 - $15.00 USD Received 29 Jan 2015; revised 11 Apr 2015; accepted 15 Apr 2015; published 21 Apr 2015

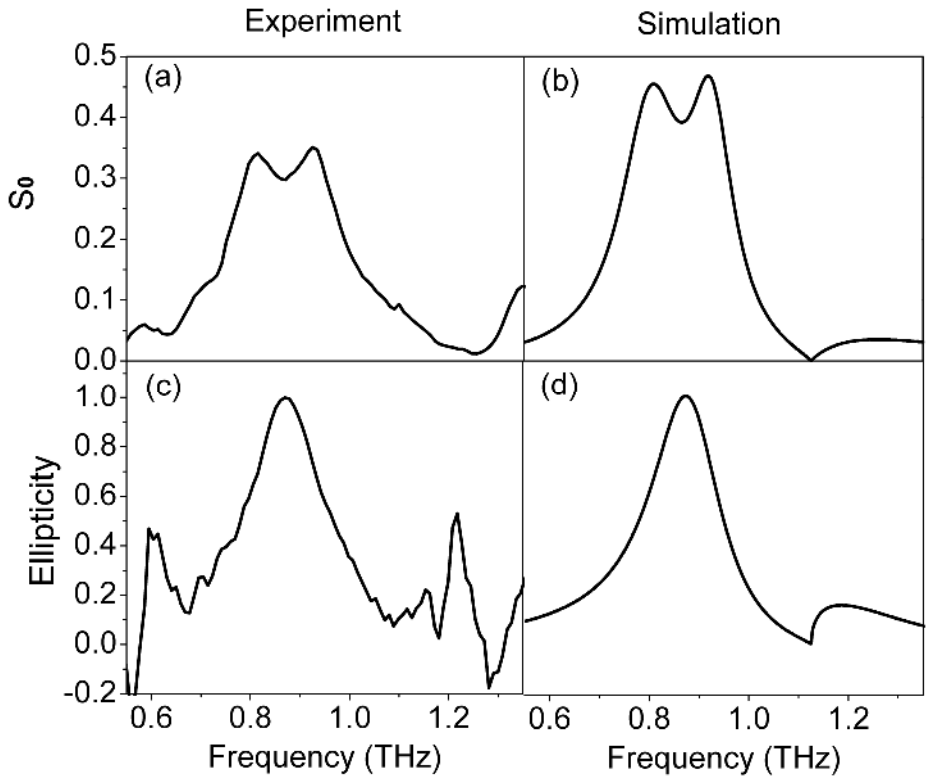

Fig. 3. (a) Measured and (b) simulated Stokes parameter S_0, and calculated ellipticities for (c) experiment and (d) simulation.

To further investigate the performance of our THz QWP, ellipticities with respect to different incident polarization angles were also calculated based on THz-TDS measured and numerical simulated results, which are shown in Fig. 4. As can be seen, when the incident polarization angle is 45 degrees, the output THz wave is a pure LCP light. When the incident polarization angle is 135 degrees, the output THz wave is a pure RCP light. This device can generate both LCP and RCP light by simply changing the incident polarization angle or, in equivalence, rotating the THz QWP. When the incident polarization angle changes to other degrees, ellipticities between 1 and −1 can be obtained. This means the output THz wave is elliptically polarized. When the incident polarization angle varies from 45 degrees to 135 degrees, the corresponding ellipticities gradually decrease from 1 to −1. Therefore, this property can be used to predict the incident polarization angle with respect to different ellipticities.

#233466 - $15.00 USD Received 29 Jan 2015; revised 11 Apr 2015; accepted 15 Apr 2015; published 21 Apr 2015

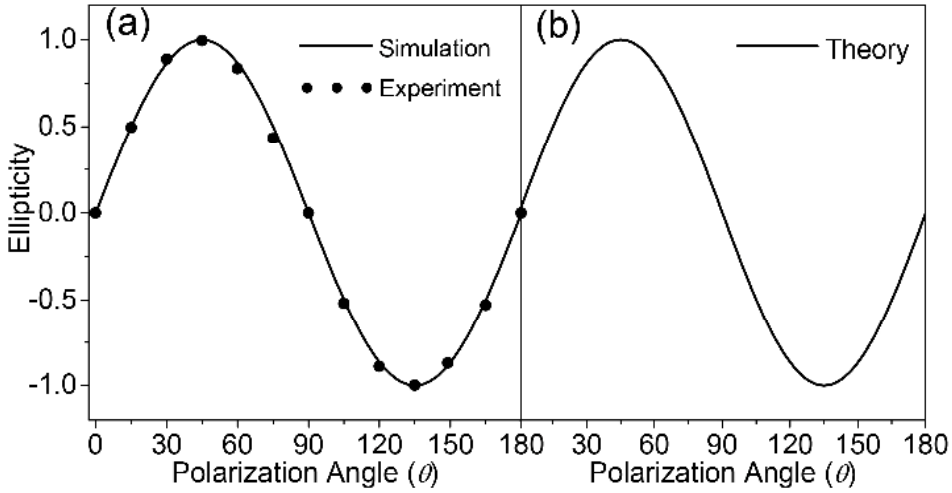

Fig. 4. (a) Measured, simulated and (b) analytical model calculated ellipticities with respect to different polarization angles of the incident wave.

4. Analytical model

For a better understanding of the physics behind the THz QWP, a Lorentz oscillator model was employed to analytically describe the transmitted amplitude, phase delay and ellipticity. Based on Babinet's principle, a slot antenna can be depicted by a Lorentz oscillator model similar to a rod antenna [43]. We can assume in our THz QWP the apertures harmonically oscillate along the incident electric field and present a transmission peak in far field. For *x* polarized incident wave, the transmitted amplitude can be described as [36]:

$$\ddot{t}_x + \gamma_x \dot{t}_x + \omega_0^2 t_x = g_x E_0 \exp(i\omega t), \tag{2}$$

where t_x and γ_x are the amplitude and damping rate of transmitted electromagnetic field. g_x is a geometric factor, revealing the coupling between the resonator and the incident electromagnetic field. ω_0 is the fundamental resonance frequency of the aperture and $E_0 exp(i\omega t)$ is the incident electromagnetic field. The solution of Eq. (2) can be derived as:

Transmitted amplitude:

$$t_x = \frac{g_x E_0}{\sqrt{(\omega_0^2 - \omega^2) + \omega^2 \gamma_x^2}}, \tag{3}$$

Phase change:

$$\tan \varphi_x = \frac{\omega \gamma_x}{\omega_0^2 - \omega^2}. \tag{4}$$

Similarly, transmitted amplitude t_y and phase change φ_y can be obtained when the incident electromagnetic wave is *y* polarized. When the incident electromagnetic wave is polarized at θ degrees to *x*-axis, the total output electric field can be treated as a superposition of two orthogonal components. With fitting parameters $g_x = 3.26$, $g_y = 3.66$ and $\gamma_x = \gamma_y = 0.75$ THz in Eqs. (3) and (4) based on the simulation results, the transmission amplitude along *x*- and *y*-axes in our THz QWP can be analytically described as shown in Fig. 2(c). A transmitted amplitude of 0.60 at 0.874 THz is presented along both *x*- and *y*-axes. The phase delay between two axes $\varphi = \varphi_y - \varphi_x$ is shown in Fig. 2(f). At 0.874 THz, the phase delay is 90

#233466 - $15.00 USD Received 29 Jan 2015; revised 11 Apr 2015; accepted 15 Apr 2015; published 21 Apr 2015

degrees, meaning the transmitted THz wave is circularly polarized. Based on the fitting results, the geometric factor g mainly depends on the resonance frequency and transmitted amplitude. In our case, the resonance frequency at 0.925 THz is larger than that at 0.806 THz. The transmitted amplitudes at two resonance frequencies are almost the same. Therefore, the corresponding geometric factor g_y is larger than g_x. The damping rates for two orthogonal slots are the same, indicating that this parameter depends on the phase delay in the slots. This is in agreement with previous reports that the length and width of metallic slots determine the propagation constants and phase delays [37, 38]. The ellipticity can also be calculated based on the superposition of these two resonant modes. As the incident THz wave is polarized at θ degrees to x-axis, the incident electric field can be described as $\bar{E} = \bar{E}x + \bar{E}y = \tilde{t}x\ cos\theta + \tilde{t}y\ sin\theta$. At the QWP working frequency, the transmitted amplitudes along x and y are the same $|\tilde{t}x| = |\tilde{t}y|$ with phase retardance of $\varphi = \varphi_y - \varphi_x = 90°$. The ellipticity $\chi = S_3/ S_0$ can be simplified as $\chi = 2sin\theta cos\theta$ based on Eq. (1). When the incident polarization angle θ changes from 0 to 180 degrees, the ellipticity can be calculated as shown in Fig. 4(b), which is in good agreement with our previous measured and simulated results shown in Fig. 4(a).

5. Conclusions

We have experimentally and numerically demonstrated an ultrathin flexible THz quarter-wave plate using asymmetric cross shape babinet-inverted metasurface. At 0.870 THz, the quarter-wave plate presents a transmitted amplitude of 0.545 along two orthogonal axes with 90 degrees phase delay and is able to convert a linearly polarized incident THz wave into a pure circular polarized light. With respect to different incident polarization angles, right-handed circular polarized light, left-handed circular polarized light and elliptically polarized light can be created flexibly. A Lorentz oscillator model is employed to analytically describe the spectral properties of the quarter-wave plate, which are in good agreement with our measured and simulated results. The planar babinet-inverted metasurface for THz polarization manipulation and the analytical model can be applied to the designs and description of novel functional THz devices and can also be extended to other frequency regimes.

Acknowledgments

This research is supported by the National Research Foundation, Prime Minister's Office, Singapore under its Competitive Research Program (CRP Award No. NRF-CRP10-2012-04).

#233466 - $15.00 USD Received 29 Jan 2015; revised 11 Apr 2015; accepted 15 Apr 2015; published 21 Apr 2015